Central European Journal of Energetic Materials
ISSN 1733-7178; e-ISSN 2353-1843

Cent. Eur. J. Energ. Mater. 2025, *22*(4): 437-469; DOI 10.22211/cejem/215528
Article is available in PDF-format, in colour, at:
https://ipo.lukasiewicz.gov.pl/wydawnictwa/cejem-woluminy/vol-22-nr-4/

Research paper

A Method for Manufacturing Solid Rocket Motor Grains Using 3D-Printed Soluble Cores

Łukasz Mężyk[1,*]), **Michał Chmielarek**[2]), **Dominik Zdybał**[1]), **Maciej Kołodziej**[1]), **Krzysztof Wacko**[1]), **Jan Kindracki**[1]), **Przemysław Woźniak**[1]), **Sylwia Metelska**[1])

[1]) *Warsaw University of Technology, Faculty of Power and Aeronautical Engineering, Institute of Heat Engineering, 21/25 Nowowiejska Street, 00-665 Warsaw, Poland*

[2]) *Warsaw University of Technology, Faculty of Chemistry, Department of High-Energetic Materials, 3 Noakowskiego Street, 00-664 Warsaw, Poland*

* *E-mail:* lukasz.mezyk@pw.edu.pl

ORCID Information:

Łukasz Mężyk: https://orcid.org/0000-0002-2297-5672
Michal Chmielarek: https://orcid.org/0000-0002-2091-4120
Dominik Zdybał: https://orcid.org/0000-0001-8965-7030
Maciej Kołodziej: https://orcid.org/0000-0002-6765-6157
Krzysztof Wacko: https://orcid.org/0000-0002-6128-6730
Jan Kindracki: https://orcid.org/0000-0002-3453-7776
Przemysław Woźniak: https://orcid.org/0000-0002-1952-0343
Sylwia Metelska: https://orcid.org/0000-0002-8269-2340

Abstract: Traditional manufacturing of solid rocket motor grains is constrained by challenges associated with the mechanical removal of the casting core. This study investigates a hybrid method that combines conventional propellant casting with 3D-printed soluble cores to overcome these manufacturing limitations and

enable greater design freedom. Moulds were fabricated using FDM from materials including BVOH, HIPS, and ABS. After casting a propellant, these moulds were dissolved using compatible solvents such as water, limonene, or acetone. The ballistic properties of the resulting propellant grains, including burn rate and ignition delay, were evaluated in a laboratory-scale rocket motor test stand. The choice of solvent proved critical to propellant performance. While organic solvents resulted in reliable ignition, water immersion caused ignition failures, likely due to the leaching of the water-soluble oxidiser. A comparison revealed that grains produced via the soluble core method exhibited a slightly higher burn rate than conventionally manufactured reference samples across a pressure range of 20 to 70 bar. The 3D-printed soluble core method is a promising technique for fabricating complex SRM grains. However, its success is critically dependent on the careful selection of a compatible material-solvent propellant system to prevent chemical interactions that degrade ballistic performance, particularly ignition reliability.

Keywords: solid rocket engine, thrust control, soluble core, additive manufacturing

1 Introduction

Shaping the thrust-time profile is one of the most critical tasks in the ballistic design of a solid rocket motor. For the chosen propellant composition, it is achieved by selecting the internal port geometry, which determines the evolution of the burning surface area A_b as a function of time. According to Vieille's burning rate law [1], the burn rate (r_b) is dependent on the chamber pressure (p) as described by the equation:

$$r_b = a \cdot p^n \tag{1}$$

where a and n are empirical constants specific to the propellant. In turn, the mass flow rate of the gases generated in combustion process ($\dot{m}$) is proportional to the burning surface area:

$$\dot{m} = A_b \, r_b \, \rho_b \tag{2}$$

where ρ_b is the propellant density. Under steady-state conditions, this mass flow is equal to the flow through the nozzle's throat. In a simplified and idealised situation, the thrust can be described as:

$$F = \dot{m} \, v_e \tag{3}$$

where v_e is exit velocity. This establishes a direct relationship between the burning surface area, chamber pressure, and the resulting thrust.

The selection of an appropriate port geometry represents a fundamental trade-off. Geometries that provide a desired thrust profile simultaneously introduce critical structural and manufacturing challenges. For example, if a neutral thrust is required, a popular star grain could be selected. However, this decision immediately creates a challenge from a structural perspective – it must be analysed whether the grain will fracture at the sharp corners of the star's points, where stress concentrations occur. Simultaneously, the problem of fabricating and safely removing the complex casting core (or mandrel) required to form such a port may occur.

This illustrates that grain design is a complex multi-criteria optimisation problem in which ballistics, mechanical integrity, and manufacturing technology are inextricably linked. The most commonly used port geometries and their effects on the motor's performance characteristics are presented in Table 1.

Table 1. The most commonly used port geometries for rocket engine motors grain [2, 3]

Name	Cross-section	Thrust profile	Key advantages	Key disadvantages/ Challenges
Cylindrical	Circular central port	Progressive	Simplicity of manufacturing, high volumetric loading fraction	Often unfavourable, increasing thrust profile
Star	Star-shaped port	Nearly neutral	Large initial burning surface area, constant thrust	Stress concentration at corners, complex core/mandrel
Finocyl	Cylinder with radial slots	Regressive/ Dual-thrust	Very high initial thrust	Complex geometry, manufacturing difficulties
BATES	Cylindrical segments	Neutral	Precise thrust profile control, simplicity of segments	Lower volumetric loading fraction, complex assembly

Traditional manufacturing technologies for propellant grains are based on three primary processes: casting, extrusion, and machining. The selection of a specific method or its combination depends on the propellant type, the required geometry, the scale of production, and safety considerations. With

the ongoing advancements in 3D printing, these techniques have also garnered attention within the field of solid propellant grain manufacturing. For high-energy materials, such as solid rocket propellants, several key 3D printing technologies have been adapted:

– Direct Ink Writing (DIW) / Paste Extrusion: It involves the precise extrusion of a propellant paste (referred to as an "ink") through a nozzle, which is deposited layer by layer to form a three-dimensional object. Piston or screw-driven systems are used for the extrusion [4, 5].
– Selective Laser Sintering (SLS): This technique involves the layer-by-layer deposition of a propellant powder and its selective sintering by a laser beam at locations corresponding to the object's cross-section. It requires exact control of the laser energy to initiate the particle sintering process without causing uncontrolled ignition of the material [6].
– Fused Deposition Modelling (FDM): This method utilises a thermoplastic filament that is melted in the print head and extruded to form an object. In propellant applications, this filament is a composite containing energetic particles within a polymer matrix. The feasibility of printing ABS-based propellants and more advanced compositions, such as the high-energy nitramine RDX in a polycaprolactone (PCL) matrix, has been investigated [7, 8].
– Vat Photopolymerization (SLA/DLP/UV-assisted): In these techniques, a liquid, photosensitive resin containing dispersed oxidiser and fuel particles is selectively cured by light (most commonly UV). These methods offer the highest resolution and surface quality. A significant advantage is their potential to replace traditional, toxic curing agents (isocyanates) with safer photoinitiators, a topic that is the subject of numerous recent patents and studies [8, 9].

This article focuses on a hybrid approach that combines the classical casting method for propellants with 3D printing techniques used to fabricate the casting moulds and the cores that shape the internal port geometry. This method has the potential to preserve the existing propellant manufacturing infrastructure without modification while simultaneously addressing the issue of costly and complex core production. A key premise of this method is the removal of the core *via* dissolution in a suitable solvent, rather than by mechanical means. Theoretically, this enables the creation of virtually any complex port geometry, including shapes that vary along the motor's axis, without the need for intricate, multi-part cores typically required for mechanical extraction. An additional goal is to use the most environmentally friendly solvent possible. However, the practical application of this method is contingent upon finding a combination of mould

material, propellant, and solvent that ensures the straightforward removal of these sacrificial cores does not alter the propellant's combustion characteristics.

2 Materials and Methods

2.1 Additive manufacturing

The first aspect was a comprehensive analysis of additive manufacturing methods, enabling the rapid and low-cost fabrication of cores with various shapes. The analysis covered different methods such as:

- Material Extrusion (ME), Fused Filament Fabrication (FFF), Fused Deposition Modelling (FDM),
- Binder Jetting (BJ),
- Material Jetting (MJ), Inkjet Printing,
- Powder Bed Fusion (PBF), Selective Laser Melting (SLM), Direct Metal Laser Sintering (DMLS),
- Vat Photopolymerization (VAT-P): Stereolithography (SLA), Continuous Liquid Interface Production (CLIP), Digital Light Processing (DLP),
- Sheet Lamination (SL),
- Direct Energy Deposition (DED), Laser Engineered Net Shaping (LENS), Directed Light Fabrication (DLF), Direct Metal Deposition (DMD), 3D Laser Cladding.

Its main objective was to examine the technology more closely in terms of its utility for the method, level of complexity, and accessibility. Simultaneously, an analysis was conducted on the materials available for use in the considered methods and the substances that could potentially serve as their solvents.

The second group of methods under consideration were solvent-free techniques. In these, the core would be removed using thermal methods. They were primarily based on the use of wax cores but were ultimately rejected due to the complex manufacturing process and thermal limitations imposed by the propellant materials themselves.

Based on the analysis, two additive techniques were selected as promising: FDM and SLA. The former utilises thermoplastic materials that are melted in the print head and cooled to solidify immediately after deposition. Objects are built up layer by layer. The SLA method utilises liquid resins that are cured with UV light. Both of these methods are relatively simple to master and inexpensive to implement. They are also relatively fast and highly flexible, both in terms of materials and the ability to make rapid changes to the core design.

One outcome of the analysis was a list of applicable materials. In both methods (SLA and FDM), material-solvent pairs were successfully identified, although for the SLA method, this choice is essentially limited to a single, water-soluble resin. For the FDM method, potentially useful materials identified included PVA, BVOH, PVB, ABS, PCL, and HIPS, along with their respective solvents such as water, alcohols, limonene, acetone, MEK, and others. This data was compiled in Table 2. A literature review on potential solvents focused on their availability, safety, and application process are compiled in Table 3.

Table 2. Materials for the chosen additive manufacturing technologies, along with potential solvents

Material	Printing technology	Commercial availability	Potential solvent	Ref.
Polyethylene oxide - Polyethylene glycol (PEO-PEG)	FDM	No	Water	[10-12]
Polyvinyl alcohol (PVA)		Yes		[13]
Butenediol vinyl alcohol copolymer (BVOH)				[14]
Polycaprolactone (PCL)			Chloroform Tetrahydrofuran Benzyl alcohol	[15, 16]
High impact polystyrene (HIPS)			Limonene	[17, 18]
Polyvinyl butyral (PVB)			Ethanol n-Propanol n-Butanol	[19, 20]
Cellulose acetate (CA)	FDM–like method	Limited	Acetone	[21]
Zortrax Z-Support ATP	FDM	Yes	Aqueous solution with an alkaline pH	[22, 23]
Zortrax Z-Support Premium			Water	[24]
Acrylonitrile Butadiene Styrene (ABS)			Acetone MEK	[25, 26]
Water soluble resin 3Dresyn IM-HDT-WS.	SLA		Water	[27]

Table 3. Various aspects of the initially proposed solvents

Solvent	Environmental aspect	Safety aspect	Process aspect
Water	Green, but concerns remain regarding energy for recycling and filament biodegradability.	Safe, but dissolved components (*e.g.* oxidisers) can pose risks.	High energy cost for recycling via evaporation due to high heat capacity. Easy to handle.
Chloroform	Toxic, suspected carcinogen, not a green solvent. Requires disposal as hazardous halogenated waste.	Highly toxic, suspected carcinogen, absorbed through skin.	Use is heavily restricted (REACH). Requires sealed systems. Storage is hazardous (can form phosgene).
Tetrahydro-furan	Flammable, toxic, and harmful to aquatic life. Not green. (2-MeTHF is a greener alternative).	Highly flammable, toxic vapours, suspected carcinogen.	A low boiling point (66 °C) is beneficial for removal but poses a high risk of fire/explosion. Can form explosive peroxides.
Benzyl Alcohol	Biodegradable and relatively safe. Considered a good „green" candidate if appropriately recycled.	Mild irritant with low vapour pressure at room temperature, but risk increases when heated.	High boiling point (205 °C) requires vacuum distillation. A good candidate for polymer separation using non-solvents.
Limonene	Green solvent from renewable sources, but toxic to aquatic life.	Skin irritant and flammable.	Moderate boiling point (176 °C) allows for simple distillation. Can precipitate polymer with alcohol addition.
Ethanol	Green solvent with negligible environmental impact.	Flammable with mildly irritating vapours.	Easy to distil. Fully miscible with water, making it versatile for various polymer recovery methods.
n-Propanol	Green solvent with negligible environmental impact.	Flammable with mildly irritating vapours.	Easy to distil and fully miscible with water.
n-Butanol	Green solvent with negligible environmental impact.	Flammable with mildly irritating vapours.	Convenient boiling point for distillation. Limited water miscibility. Must be protected from oxidation.

2.2 Propellant grain

In parallel with the review of 3D printing materials and techniques, an analysis of potential propellant compositions was conducted, taking into account the feasibility of their in-house manufacturing at the Warsaw University of Technology. The primary focus was placed on composite solid propellants.

The fundamental components of composite solid rocket propellants are solid crystalline oxidiser particles and a binder, which also serves as the fuel. This binder acts as a matrix that encapsulates and uniformly disperses the solid oxidiser. The choice of binder has a significant influence on the propellant's physical properties, including its rheology and mechanical strength. The type of polymer matrix – which can be based on hydroxyl-terminated polybutadiene (HTPB), carboxyl-terminated polybutadiene (CTPB), polybutadiene acrylonitrile (PBAN), or energetic polymers like glycidyl azide polymer (GAP) – is selected based on processing ease, cost, application, and the required burn rate. The chemical curing of a liquid synthetic polymer typically forms this matrix. The most common system in rocket propellants is HTPB, which is cured with isocyanates (such as TDI or HDI) to form a polyurethane network.

The oxidiser, such as ammonium perchlorate (AP), ammonium nitrate (AN), potassium nitrate (KN), or ammonium dinitramide (ADN), functions as the filler. In addition to the oxidiser, binder, and metal powders, composite propellants contain other components, including plasticisers, curing catalysts, ballistic modifiers, antioxidants, and bonding agents. The types and amounts of these additives can be modified to achieve the desired propellant properties. During manufacturing, the oxidiser is introduced at an elevated temperature (50-80 °C) into the liquid binder, plasticiser, and curing agent, which then solidifies to form the composite grain. The solid particles can constitute up to 89% of the propellant's total mass. The typical components of composite solid propellants, along with their respective mass percentage ranges, are summarised in Table 4.

Table 4. Typical components of composite solid rocket propellants

Function	Ingredient	Amount [%]
Oxidizer	AP, AN, ADN, KN	0-70.0
Binder (fuel)	HTPB, CTPB, HTPE, HTPS, PBAN, PU	0-18.0
Energetic binder (fuel)	GAP, AMMO, BAMO, BTTN, TEGDN, TMETN	0-14.0
Curing agent / Hardener	IDPI, HDI, MAPO, TDI	0.2-3.5
Burn rate catalyst	Fe_2O_3, FeO, ferrocene and its derivatives	0.2-3.0
High-energy additive	RDX, HMX, ADN, NQ	0-40.0
Bonding agent / Coupling agent	MAPO, Hx-752	a fraction of a percent
Plasticizer	DOP, IDP, DOA	0-7.0
Metal powder	Al	0-30.0
Burn rate modifier	Zr, ZrC, Al	a fraction of a percent

In the proposed method, the propellant comes into direct contact with the solvent used for extracting the core or the entire mould. It was therefore necessary to investigate the solubility of standard propellant components in the potential solvents to assess any adverse effects. Using literature data [28, 29, 30-41] and the Safety Data Sheets (SDS) of each ingredient, a solubility matrix was established and delivered in Table 5.

Table 5. Solubility matrix of common rocket propellant components in chosen solvents

Component / Solvent	Water	Chloroform	THF	Benzyl alcohol	Limonene	Ethanol	n-Propanol	n-Butanol	Acetone	NaOH (aq)
HTPB	No	Yes	Yes	N/D	N/D	Yes	Yes	Yes	Yes	No
GAP										
AP	Yes	No	No			No	No	No	No	Yes
Al	No									NO
Hx-752		N/D	N/D			N/D	N/D	N/D	N/D	N/D
MAPO		Yes	Yes			Yes	No	No	NO	No
TDO				Yes		No			Yes	
SDO										
ADO										
TMETN				N/D		Yes	Yes	Yes		
IPDI				No		No	No	No		
HDI										
DDI										
Ferrocene				Yes		Yes	Yes	Yes		
Catocene										
Fe_2O_3		No	No	No		No	No	No	No	
Cr_2O_3										
BEFPO		Yes	Yes	Yes		Yes	Yes	Yes	Yes	
Fc-HTPB				N/D						

Table 6. Compositions of propellants tested at Warsaw University of Technology

Propellant	HTPB	Fc-HTPB	AP	Al	Hx-752	ADO	TMETN	IPDI	Ferrocen	Katocen	Fe_2O_3	Cr_2O_3	Nano Fe_2O_3	BEFPO
B-1	12	–	80	–	0.5	5	–	2.5	–	–	–	–	–	–
B-2			79						1					
B-3			78						2					
B-4			77						3					
B-5			79						–	1	–			
B-6			78							2				
B-7			77							3				
B-8			79							–	1			
B-9			78								2			
B-10			77								3			
B-11			79								–	1	–	
B-12			78									2		
B-13			77									3		
B-14			79									–	1	
B-15			78										2	
B-16			77										3	
B-17			79									–	–	1
B-18			78											2
B-19			77											3

Table 6. Continuation

Propellant	HTPB	Fc-HTPB	AP	Al.	Hx-752	ADO	TMETN	IPDI	Ferrocen	Katocen	Fe_2O_3	Cr_2O_3	Nano Fe_2O_3	BEFPO
B-20	12	–	64	15	0.5	5	–	2.5	1	–	–	–	–	–
B-21			63						2					
B-22			62						3					
B-23			64						–	1				
B-24			63							2				
B-25			62							3				
B-26			64							–	1	–		
B-27			63								2			
B-28			62								3			
B-29			64								–	1		
B-30			63									2		
B-31			62									3		
B-32			64									–	1	–
B-33			63										2	
B-34			62										3	
B-35			64								–		–	1
B-36			63									–		2
B-37			62											3
B-38	11.4	0.6	80	–										–
B-39	10.8	1.2	80											
B-40	10.2	1.8	80											

The use of solvents to remove the mould from a cured rocket propellant carries the risk of damaging the propellant's matrix. Each solvent has the potential to dissolve and leach specific components from the polymer matrix. This vulnerability primarily affects the oxidiser, burn rate catalysts, and processing aids. The main structural components – the polymer and the isocyanate curing agent – react to form a polyurethane binder that is resistant to the selected solvents.

Experimental studies on mould removal should begin with materials soluble in water. A review of the properties of raw materials used in solid composite rocket propellants indicates that water is incapable of dissolving and leaching out the burn rate catalysts. Furthermore, the polyurethane formed from the reaction of GAP or HTPB with an isocyanate should protect the oxidiser. The cast

propellant grain has a thin polyurethane film on its external surfaces. Assuming the hydrophobic properties of HTPB- or GAP-based polyurethanes prevent water from penetrating the propellant's matrix, the leaching of components should not occur. However, if this polyurethane layer is breached, water would likely only leach the oxidiser from the exposed surface of the propellant sample.

In contrast, the action of organic solvents can be more invasive and may damage the propellant's internal structure. However, only experimental testing will verify the feasibility of their use. Organic solvents can leach components that are used in amounts not exceeding 5% of the total propellant mass. Leaching even a fraction of such a component from the sample's surface could have a significant impact on the rocket propellant's properties.

3 Experiments

3.1 Sample preparation

The initial stage of the experimental work involved selecting a baseline geometry for the propellant grain, which subsequently determined the configuration of the core. A primary design constraint was the necessity for the grain to be compatible with the existing test stand at the Institute of Heat Engineering, where the ballistic evaluations were to be performed. Furthermore, safety considerations imposed limitations on the maximum permissible sample size.

Accordingly, a cylindrical grain geometry was established as the baseline configuration, featuring an outer diameter of 16 mm and a central cylindrical port with a diameter of 8 mm. The propellant samples were cast to an approximate length of 35 mm and subsequently machined to a final length of 15 mm for the investigation. The figure below illustrates exemplary moulds fabricated from three distinct materials.

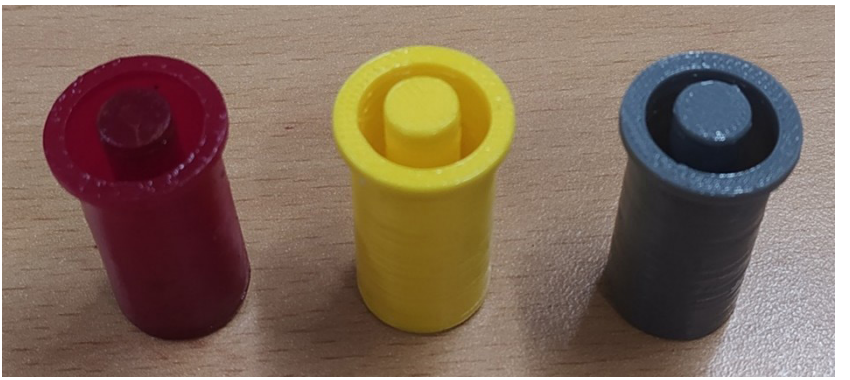

Figure 1. Individual moulds were made from three different materials: a water-soluble resin, ABS, and HIPS

The moulds were evaluated based on their dissolution time. The results indicated that approximately 4 h of immersion in a suitable solvent was sufficient for the complete dissolution of the mould.

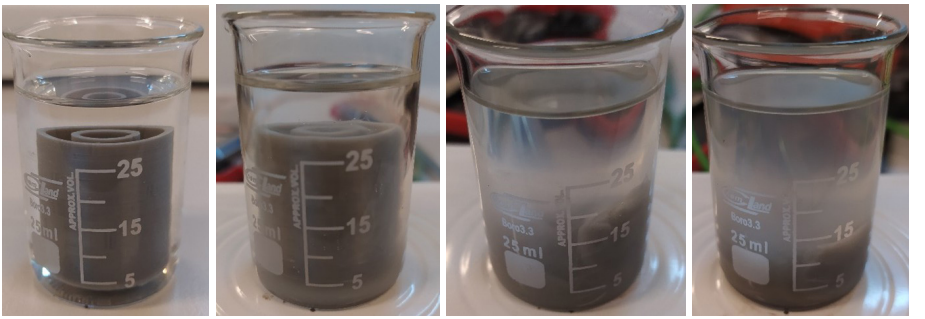

(a) (b) (c) (d)

Figure 2. The dissolution process of a HIPS mould in Limonene: images depict, respectively, the initial state (a) and the state after exposure to the solvent for 1.5, 2.5 and 4.5 h, (b)-(d), respectively

Propellant samples manufactured via the conventional method were also subjected to four-hour immersion tests to observe any potential degradation. Upon removal from the solvents, a distinct visual effect was observed, which was a change in the samples' dimensions. While the samples retained their structural integrity and shape, they exhibited swelling, which was attributed to the absorption of the solvent. A visual comparison of the samples is presented in Figure 3.

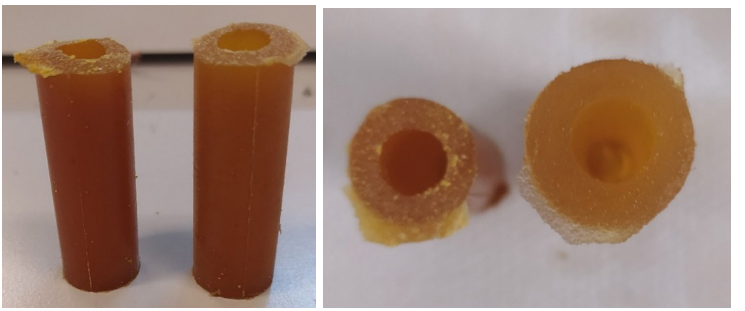

Figure 3. Comparison of an untreated sample (left) with a solvent-immersed sample (right)

Since dimensional change in the propellant grain is an undesirable effect, the samples were subjected to a vacuum treatment for approximately 24 h. This procedure enabled the samples to revert to their initial dimensions. It was noted, however, that this treatment must be performed immediately upon removal of the samples from the solvent. Samples that underwent the vacuum process after a time delay retained their deformed state.

A simple investigation was conducted to determine whether the samples retained their flammability (under ambient atmospheric conditions) after solvent immersion. For this purpose, discs with a thickness of 5 mm were prepared and subsequently immersed for 4 h in a selection of baseline solvents: water, MEK, and Limonene, chosen due to their availability and "green" potential. Subsequently, each disc was combusted in a designated setup, consisting of a fume hood equipped with an exhaust system and a steel combustion dish. Video recordings were made to facilitate qualitative observation of the combustion event, including the volume of smoke produced, as well as the approximate duration and dynamics of the burning process. Ignition of the samples was performed using a gas igniter. A sequence from a single trial is presented in Figure 4.

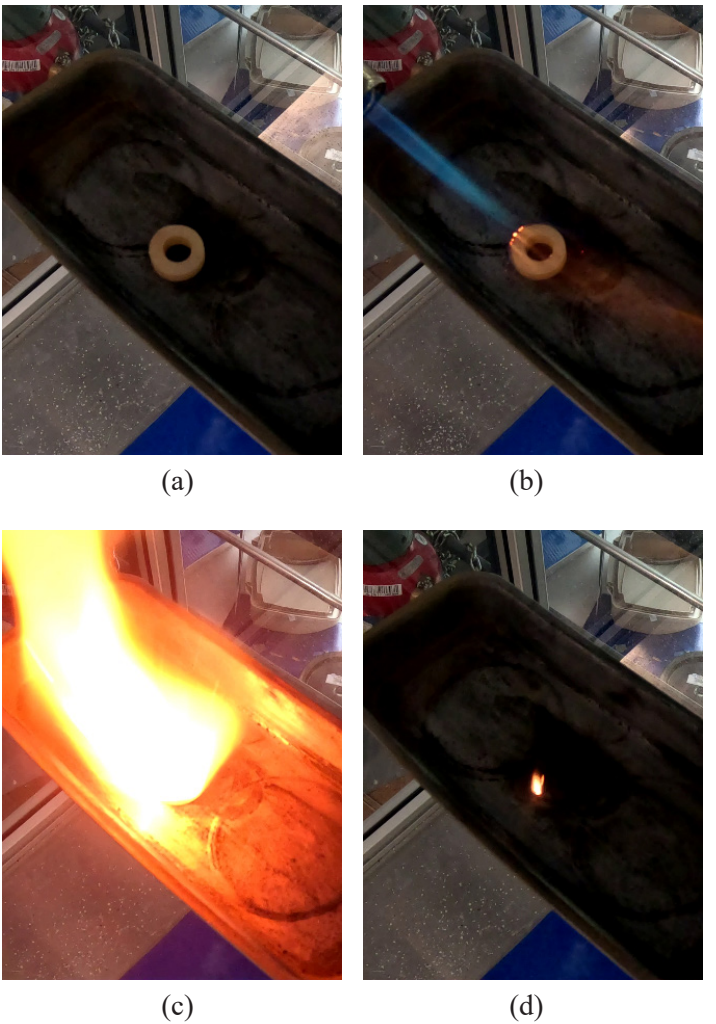

Figure 4. An exemplary sequence of an experiment investigating the flammability retention of a propellant sample following solvent immersion: sample ready for combustion (a), ignition (b), main combustion (c) and afterburning (d)

All the tested samples made of the chosen materials (propellants: B3, B-15, B-14, as listed in the table) retained their ability to combust. It was observed, however, that virtually all of them exhibited a lower burn rate compared to the untreated samples. Additionally, they emitted an increased volume of smoke during combustion.

Following these preliminary experiments, the investigation proceeded to tests conducted in a laboratory-scale rocket motor. For this purpose, propellant samples were prepared by casting them into moulds printed from the previously mentioned materials. These cast samples were then placed in vessels containing the respective solvents, and the liquid was agitated using a magnetic stirrer. An example of this mould extraction process is illustrated in Figure 5. Another examples of some propellant - mould material – solvent are presented in Figure 6.

(a)

(b)

(c)

Figure 5. Exemplary mould extraction process (mould material: HIPS): the propellant sample cast in the mould (a), samples prepared for the dissolution process (b) and the propellant grain immediately after mould dissolution (c)

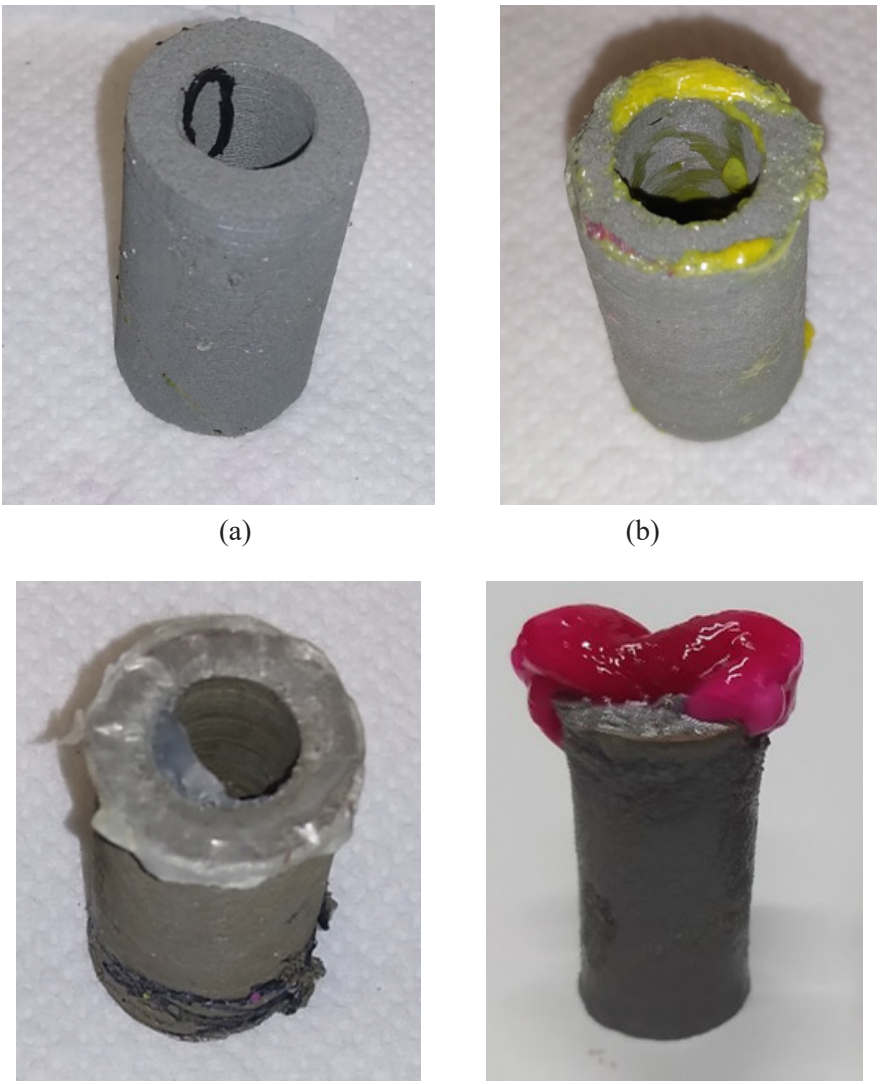

(a) (b)

(c) (d)

Figure 6. Results of mould dissolution of samples: a) B23 – BVOH/H_2O (a), B24 – ABS/acetone (b), B20–HIPS – Limonen (c) and B20–Soluble resin – H_2O (d)

3.2 Laboratory stand

The laboratory test stand, designed for the combustion testing of samples under simulated rocket motor conditions, is depicted in Figure 7.

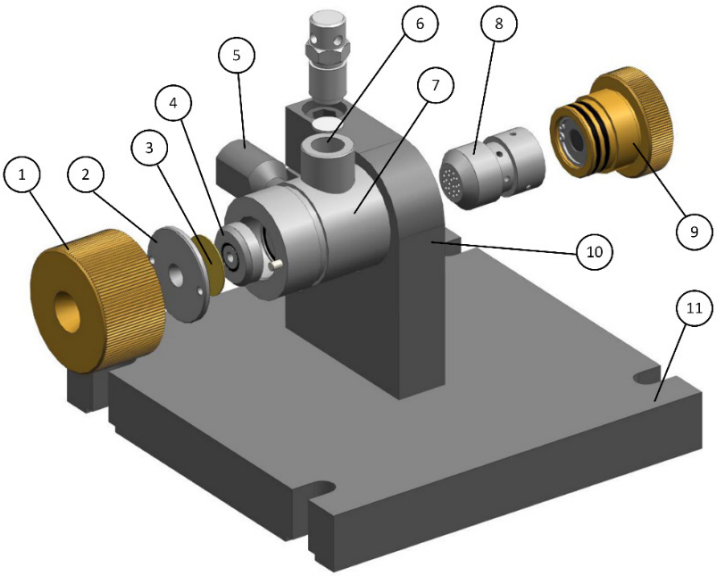

Figure 7. Test stand for propellant burn rate determination: 1 – nozzle assembly retainer, 2 – diaphragm retainer, 3 – nozzle diaphragm, 4 – nozzle insert, 5 – pressure transducer port, 6 – safety valve port, 7 – combustion chamber, 8 – propellant grain holder, 9 – igniter assembly, 10 – combustion chamber mount and 11 – test stand base

The primary component of the test stand is the combustion chamber, which is secured in a mount and firmly affixed to the laboratory bench by the stand's base. The chamber is equipped with a detachable transducer that records the pressure profile during operation. This transducer is threaded into a dedicated port and is shielded from the corrosive chemical effects of combustion gases by a replaceable layer of silicone grease. This design allows for the measurement of gas pressure without direct contact between the gases and the transducer's diaphragm.

The chamber also features a port for a safety valve that operates on the principle of a burst diaphragm. Upon reaching pressures considered hazardous for the apparatus, the diaphragm instantly ruptures, releasing the gases into the surroundings and thereby protecting the test stand from damage. The material and thickness of the diaphragm were determined experimentally, tailored to the specific tasks being performed.

The chamber is sealed on one end by a nozzle assembly, which consists of a nozzle insert, a diaphragm, a diaphragm retainer, and a nozzle assembly retainer. The nozzle diaphragm is a standard component in solid propellant

motors, facilitating a slight pressure increase within the combustion chamber upon ignition, which promotes better ignition conditions. Its material and thickness can be adjusted depending on the desired operating pressure initiation. Although not always necessary, a single-layer paper tape diaphragm was used in these experiments to maintain a consistent testing standard.

The nozzle insert is the component that defines the critical cross-section (throat), which in turn determines the pressure at which the propellant will combust. The interchangeable design of the nozzle insert allows for changes to the throat area, enabling tests under various pressure conditions. This is also important for minimising the production costs of the entire nozzle. The throat area is highly susceptible to erosion, necessitating frequent replacement to maintain consistent geometric conditions. Replacing the entire nozzle would be costly; since the nozzle insert is a geometrically simpler component, its use significantly reduces experimental costs. The throat orifices can be manufactured in any size permitted by the available machinery.

The propellant grain – a cylinder 16 mm in diameter and 15 mm in length with a single 8 mm central port – was placed in the propellant grain holder and then inserted together into the combustion chamber. The chamber is closed by the igniter assembly, which consists of an electric initiator (Nitroerg SA, Poland) with a safe current of 200 mA and a 0.5-gram booster charge of loose black powder, all housed in a threaded enclosure. Ignition is initiated by supplying power from the control system to the igniter, which in turn ignites the black powder. The resulting hot gases and solid particles make direct contact with the propellant grain, inducing its ignition.

The entire process is controlled automatically by a computer, which is also responsible for data acquisition and processing. To ensure the safe execution of experiments, the system is equipped with a three-stage safety mechanism that allows the researcher to leave the potential hazard zone. This safety system includes a timer that delays the signal sent to the igniter after the sequence is initiated, as well as two physical switches that prevent signal transmission when open. This setup enables the experimenter to prepare and initiate the sequence safely, then retreat to a separate room for the duration of the combustion process.

Data registration includes recording the pressure profile in the combustion chamber, the igniter activation signal, and, additionally, the voltage and current profiles of the ignition circuit. This data allows for the determination of the burn rate and ignition delay. To evaluate the propellant's burn rate, the 50% maximum pressure method was adopted. This means that the burn time is calculated as the interval from the moment the pressure reaches half its maximum value on the rising curve to the moment it falls to the same value on the decaying curve.

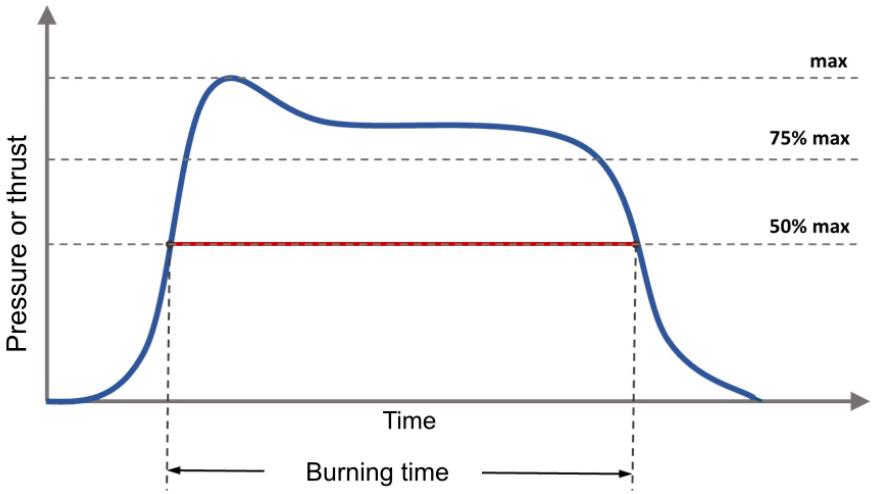

Figure 8. Principle of sample burn time determination in the test motor

4 Results

Subsequently, combustion tests were performed in a test motor using three different propellants, which were available at the time – B20, B22, and B23 – in moulds manufactured from BVOH, HIPS, and ABS. A representative complete result for a single experiment is presented in Figure 9. Data acquisition was conducted for 10 s, but the graph displays data only within the region of interest. The red curve, labelled "pressure," represents the pressure profile within the combustion chamber. A sudden pressure spike is observed, resulting from the activation of the ignition system. This is followed by a slightly slower pressure rise due to the combustion of the prominent propellant grain. "Trigger" indicates the moment the signal is issued to activate the igniter. "Current" (an extremely brief period) is the duration of the current flow through the ignition system until the igniter burns out. The ignition delay time is defined as the time interval between igniter activation and reaching 50% of the maximum pressure during the combustion of the main propellant. Depending on material availability, 2 to 4 experiments were performed for each combination of propellant, mould and solvent. Representative comparison of pressure traces for one type of material is presented in Figure 10.

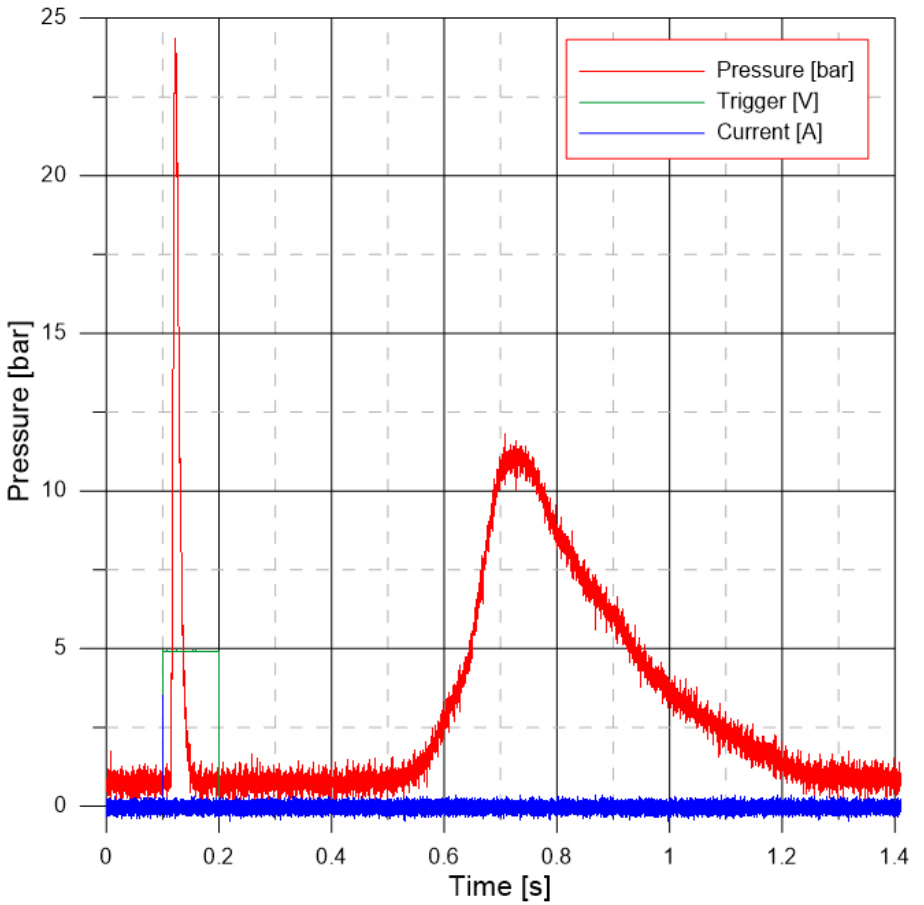

Figure 9. An exemplary result of an experiment

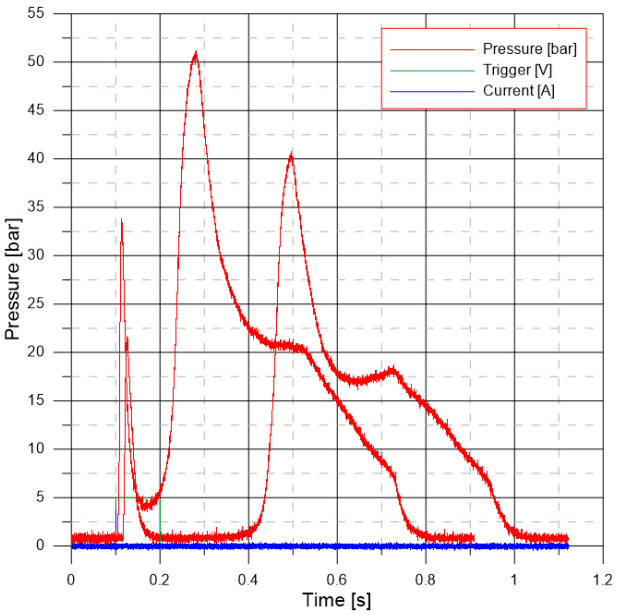

(a)

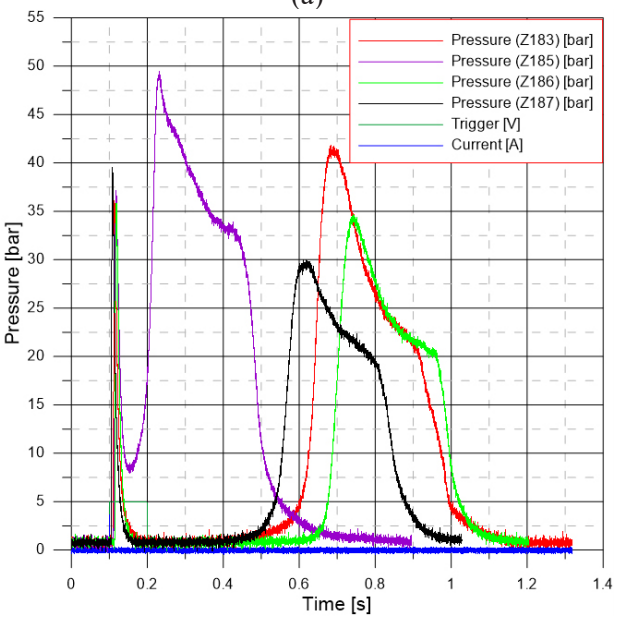

(b)

Figure 10. Pressure traces for B20 material prepared with: the traditional method (a) and a mould made of HIPS dissolved in limonene (b)

Once the data were acquired, they were processed using a semi-automated script written in the MATLAB environment. The script's primary function was to identify characteristic points and calculate the corresponding discrete data points and specific average values.

The plots present the propellant's burn rate and the ignition delay time as the most characteristic features for solid propellant. Each plot contains data for a single propellant type, showing results for all the different solvents used for mould removal.

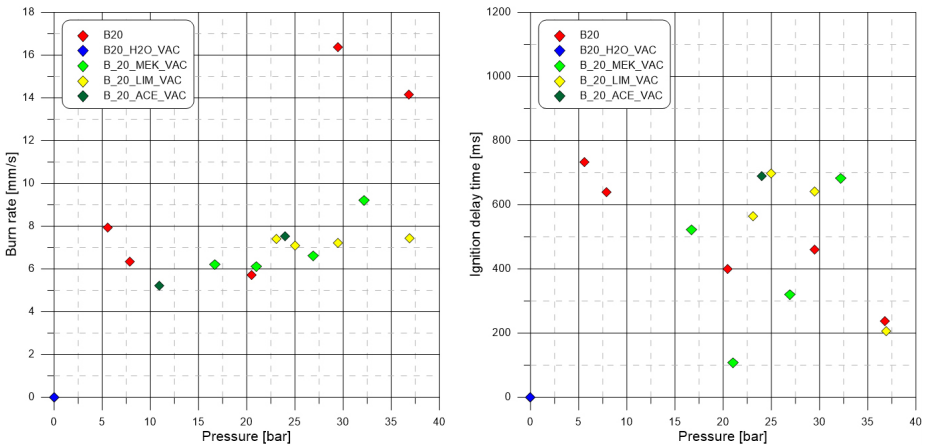

Figure 11. Burn rate and ignition delay time as a function of pressure for the B20 propellant, showing results for various mould materials

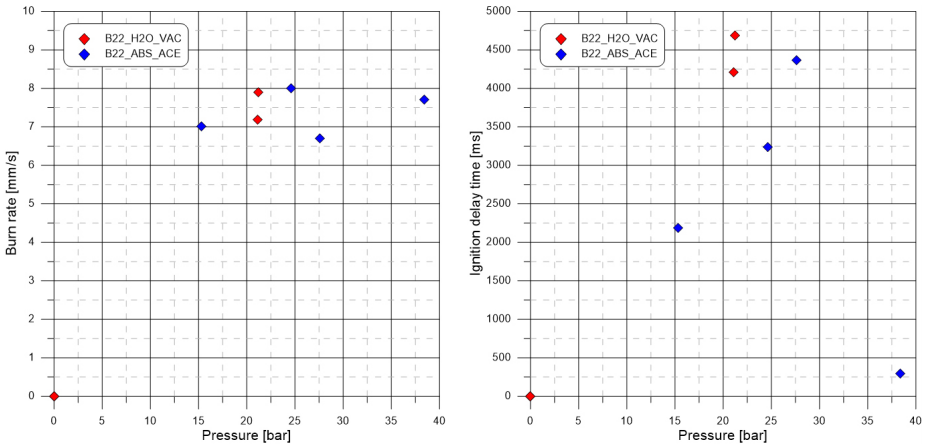

Figure 12. Burn rate and ignition delay time as a function of pressure for the B22 propellant, showing results for various mould materials

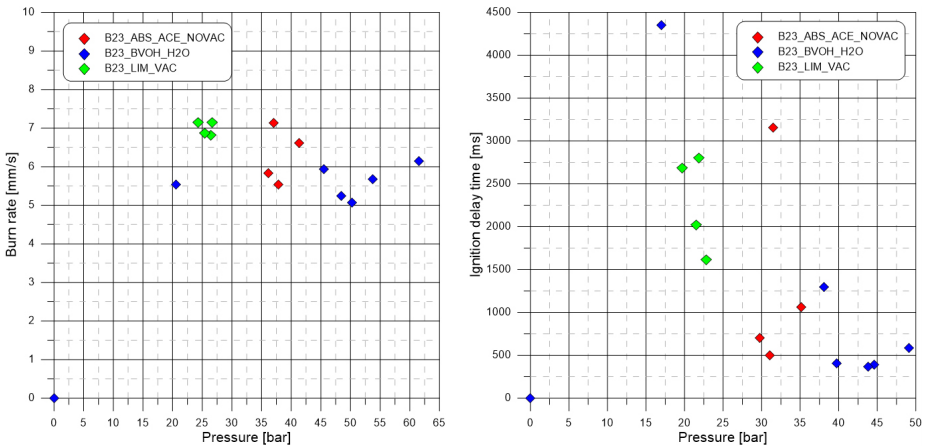

Figure 13. Burn rate and ignition delay time as a function of pressure for the B23 propellant, showing results for various mould materials

Due to the large number of variable combinations but a small number of samples for each, it was not possible to determine the burn rate laws from the experimental results obtained. Establishing these laws would require a greater number of repetitions and a wider range of pressure conditions within the combustion chamber. Therefore, the decision was made to prepare a subsequent batch of propellant. A propellant with formulation B1 was selected, and samples were fabricated by casting into water-soluble BVOH moulds. Water was chosen despite previous observations about its influence on an ignition event due to safety reasons. Concurrently, samples of the same geometry were produced using the conventional method (a removable steel core).

(a)

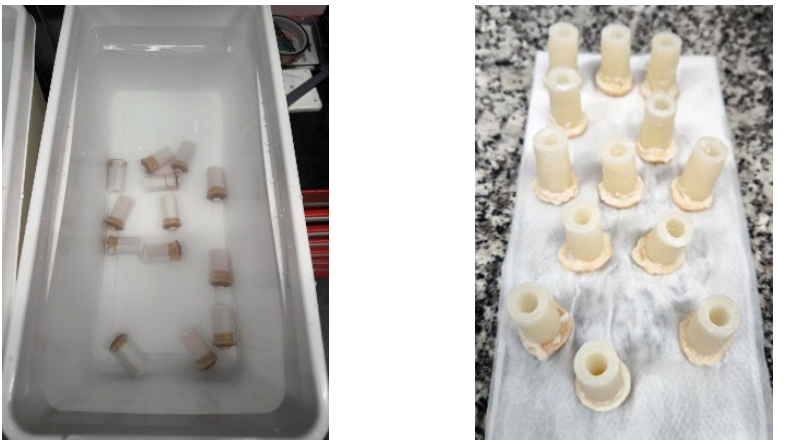

(b) (c)

Figure 14. B1 propellant: cast in BVOH made moulds (a), during mould dissolving in water (b) and after mould removal (c)

The experiments were conducted on the same test stand and in the same manner as previously described, with the sole difference being the use of nozzle inserts with varying throat cross-sections to generate a range of combustion chamber pressures. Tests were performed using inserts with throat diameters of 2.4, 2.6 and 2.8 mm, resulting in chamber pressures in the range of 20-70 bar. Four experimental runs were conducted for each nozzle insert size.

An identical procedure was applied to the propellant manufactured via the conventional method. The outcome of this investigation was the characterisation of the burn rate as a function of chamber pressure for the propellants produced by both manufacturing techniques. These two relationships were subsequently compared in Figure 15.

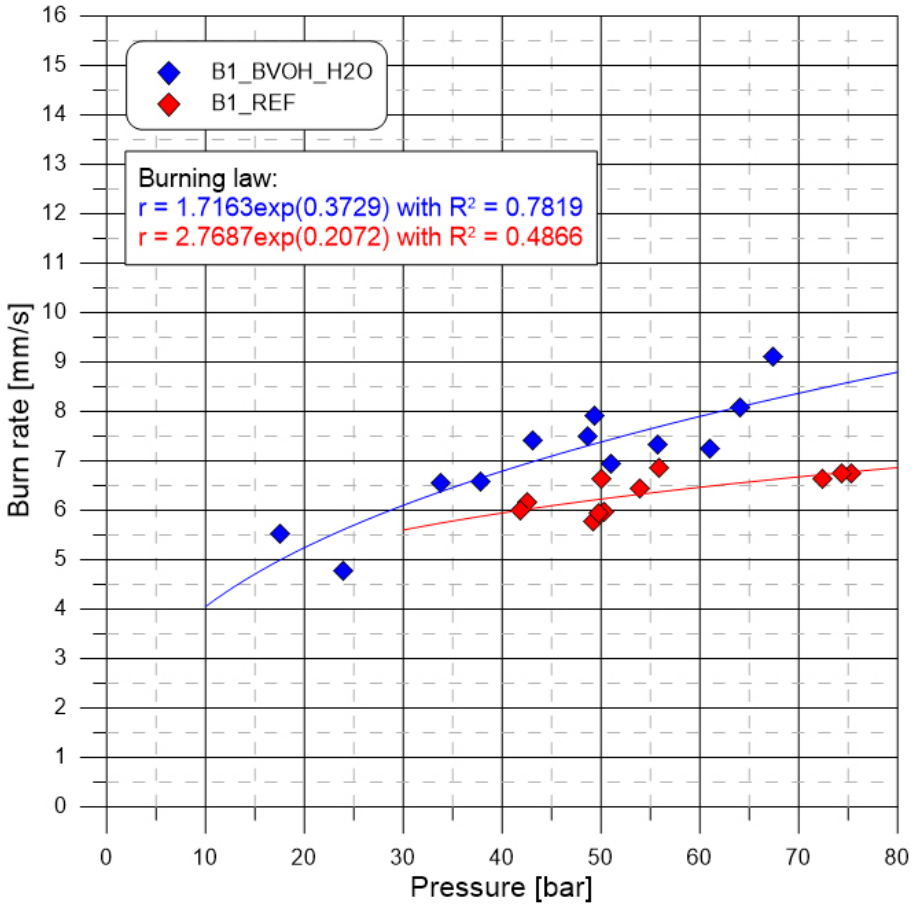

Figure 15. Results of the experimental determination of the burn rate law for propellant B1, comparing samples prepared *via* the conventional and soluble core methods

According to the obtained results, samples produced by the soluble core method burn more quickly compared to those produced by the conventional method. This result is somewhat surprising, considering the information gathered in the previous stage of the research. Furthermore, the experimental results for the new method also align with a more clearly defined trend line. It should be noted, however, that the coefficient of determination (R^2) for the curve fit remains low in both cases. This leads to the conclusion that the current results exhibit limited repeatability. To improve the precision of the determined burn

rate law, a greater number of experiments should be conducted across a wider pressure range. Two potential causes are proposed to explain the increased burn rate observed in the water-immersed samples.

The first hypothesis relates to the vacuum treatment applied during sample preparation. The manufacturing process for the soluble core method involved subjecting the propellant grains to a vacuum after core dissolution to restore their initial shape, even when deformation from liquid contact was minimal. This step could have introduced a degree of surface porosity, which would, in turn, influence the burn rate by unexpectedly increasing the combustion surface area. This post-curing vacuum treatment was not performed on the samples produced by the conventional method. While the conventional casting process itself occurs under vacuum, the fully cured grains were not subjected to this secondary vacuum exposure.

A second explanation could be the inherent difficulty in igniting the grains manufactured via the conventional method. During the curing process, a thin layer of pure polymer forms on the surfaces that are in contact with the mould, which hinders ignition. This is a particular issue for small samples, such as those used in this study, where the limited surface area and brief contact time with the igniter's combustion products can be critically affected by the presence of this inhibitive layer. In this investigation, the conventionally produced reference samples exhibited significant ignition problems. To improve their ignitability, the surfaces were manually treated by abrading them with wire brushes to disrupt the polymer layer.

Both effects – potential porosity from the vacuum process and differences in surface preparation – may be particularly significant at the small geometric scale of the samples tested. Therefore, further investigations on a larger scale (calibre) are planned for future work to clarify these phenomena.

5 Summary

- This paper presents a method for manufacturing solid rocket motor (SRM) grains using 3D-printed soluble cores, a technique designed to overcome the limitations of traditional mechanical core removal, particularly for complex grain geometries. The study utilises accessible additive manufacturing technology, Fused Deposition Modelling (FDM), to fabricate cores from materials such as HIPS, ABS, and water-soluble BVOH. After the propellant is cast and cured, the core is dissolved in a compatible solvent, such as limonene, acetone, or water.

- The experimental phase focused on HTPB/AP-based propellants. An initial investigation into the solvent's effect on the propellant revealed that while immersion could cause reversible swelling (rectified by vacuum treatment), it also tended to lower the burn rate and increase smoke production compared to untreated samples.
- Ballistic tests in a laboratory-scale rocket motor revealed that while the vast majority of samples ignited successfully, the choice of solvent was critical. Water-immersed samples posed significant challenges; for propellant B-20, no successful ignition data was recorded, with two samples failing to ignite and two others experiencing delays (4-6 s) that exceeded the initial data acquisition window. Propellant B-22 also showed a high ignition failure rate with water (3 out of 5 attempts failed). In contrast, organic solvents like MEK, limonene, and acetone resulted in reliable ignition across all tested propellants. This suggests a potential incompatibility, likely the leaching of the water-soluble AP oxidiser, which compromises ignition performance.
- Analysis of the burn rate data from these initial tests was complicated by considerable data scatter and a lack of repeatability, which was attributed to the large number of variables and the limited number of samples for each configuration. This prevented the determination of precise burn rate laws. However, a counterintuitive trend was observed for propellant B-23, where samples treated with limonene exhibited the highest burn rates at the lowest pressures, contrary to the expected relationship, revealing a potential influence of the solvent.
- To overcome these limitations, a subsequent, more controlled experiment was conducted. A single propellant formulation (B1) was manufactured using both the new method (with water-soluble BVOH cores) and the conventional method (with a removable steel core). By testing these samples with nozzle inserts of varying throat diameters (2.4, 2.6 and 2.8 mm), a range of operating pressures (20-70 bar) was achieved, allowing for the successful characterisation of the burn rate law for both manufacturing techniques. The results from this final phase indicate a slightly lower burn rate for the conventionally manufactured propellant compared to the propellant produced using the soluble core method across the tested pressure range.
- In conclusion, the 3D-printed soluble core method is a viable and promising technique that offers significant design freedom for complex solid rocket engine grains; however, it requires further detailed research and some improvements. Its implementation requires careful selection of a material-solvent-propellant system to avoid adverse chemical interactions that can negatively impact ballistic performance, particularly ignition reliability.

As an extension of this work, the authors plan to conduct further experiments using limonene and water as the solvents. These future investigations will be performed at an elevated temperature. They will incorporate a flow-through mould dissolution system to reduce the potential contact time between the propellant grain and the solvent.

Acknowledgements

Research was funded by Warsaw University of Technology within the Excellence Initiative: Research University (IDUB) programme.

References

[1] DeLuca, L.T.; Galfetti, L.; Colombo, G.; Maggi, F.; Bandera, A.; Babuk, V.A.; Sinditskii, V.P. Microstructure Effects in Aluminized Solid Rocket Propellants. *J. Propuls. Power* **2010**, *26*(4): 724-733; https://doi.org/10.2514/1.45262.

[2] Sutton, G.P.; Biblarz, O. *Rocket Propulsion Elements*. 9th ed., John Wiley & Sons, Hoboken, **2017**; ISBN: 978-1-118-75365-1.

[3] Mallela, P.R.S.; Aravind, S.; Rathi, N.; Yadav, D.P.R.; Ramakrishna, P.A. Processing and Testing Subscale Motors with Central Finocyl Grain Using Wax Mandrel. *J. Propuls. Power* **2025**, *41*(3): 381-387; https://doi.org/10.2514/1.B39667.

[4] Chandru, R.A.; Balasubramanian, N.; Oommen, C.; Raghunandan, B.N. Additive Manufacturing of Solid Rocket Propellant Grains. *J. Propuls. Power* **2018**, *34*(4): 1090-1093; https://doi.org/10.2514/1.B36734.

[5] Song, S.; Shi, J.; Ren, Q.; Miao, K.; Tang, M.; Shi, H. Comparative Study on Extrusion 3D Printing of Solid Propellant Based on Plunger and Screw. *Materials* **2025**, *18*(4) paper 777; https://doi.org/10.3390/ma18040777.

[6] Brown, C.B.; Chewakin, E.; Feldman, M.; Lima, A.; Lindholm, N.; Lipscomb, C.; Niedzinski, R.; Sobol, J. *Solid Propellant Additive Manufacturing (SPAM)*. Report, University of Colorado at Boulder Aerospace Engineering Services, **2017**; https://www.colorado.edu/aerospace/sites/default/files/attached-files/spam_aiaa.pdf [accessed on Oct. 10, 2025].

[7] *3D Printed Rocket Thrusters Could Change Small Spacecraft Industry*. 3DPrint.com, **2018**; https://3dprint.com/208635/3d-printed-rocket-thrusters/ [accessed on Oct. 10, 2025].

[8] Zhang, J.; He, K.; Zhang, D.; Dong, J.; Li, B.; Liu, Y.; Gao, G.; Jiang, Z. Three-Dimensional Printing of Energetic Materials: A Review. *Energ. Mater. Front.* **2022**, *3*(2): 97-108; https://doi.org/10.1016/j.enmf.2022.04.001.

[9] Benali, F.; Shpilman, Z.; Dorfman, S.; Sudry, Y.; Weihs, D. Composite Propellant Manufacturing Process Based on Deposition and Light-activated Polymerization for Solid Rocket Motors. *Def. Technol.* **2020**, *16*(4): 861-867; https://doi.org/10.1016/j.dt.2019.10.009.

[10] Özdemir, C.; Güner, A. Solubility Profiles of Poly(Ethylene Glycol)/Solvent Systems, I: Qualitative Comparison of Solubility Parameter Approaches. *Eur. Polym. J.* **2007**, *43*(7): 3068-3093; https://doi.org/10.1016/j.eurpolymj.2007.02.022.
[11] Zustiak, S.P.; Leach, J.B. Hydrolytically Degradable Poly(Ethylene Glycol) Hydrogel Scaffolds with Tunable Degradation and Mechanical Properties. *Biomacromolecules* **2010**, *11*(5): 1348-1357; https://doi.org/10.1021/bm100137q.
[12] Isreb, A.; Baj, K.; Wojsz, M.; Isreb, M.; Peak, M.; Alhnan, M.A. 3D Printed Oral Theophylline Doses with Innovative 'Radiator-like' Design: Impact of Polyethylene Oxide (PEO) Molecular Weight. *Int. J. Pharm.* **2019**, *564*: 98-105; https://doi.org/10.1016/j.ijpharm.2019.04.017.
[13] *Water Soluble Filament: Properties, How to Use, and Best Brands*. 3D Insider, **2019**; https://3dinsider.com/water-soluble-filament/ [accessed on Oct. 10, 2025].
[14] Jung, B.N.; Kang, D.H.; Shim, J.K.; Hwang, S.W. Physical and Mechanical Properties of Plasticized Butenediol Vinyl Alcohol Copolymer/Thermoplastic Starch Blend. *J. Vinyl Addit. Technol.* **2019**, *25*(2): 109-116; https://doi.org/10.1002/vnl.21621.
[15] Azimi, B.; Nourpanah, P.; Rabiee, M.; Arbab, S. Poly (ε-Caprolactone) Fiber: An Overview. *J. Eng. Fiber Fabr.* **2014**, *9*(3): 74-90; https://doi.org/10.1177/155892501400900309.
[16] Ntrivala, M.A.; Pitsavas, A.C.; Lazaridou, K.; Baziakou, Z.; Karavasili, D.; Papadimitriou, M.; Ntagkopoulou, C.; Balla, E.; Bikiaris, D.N. Polycaprolactone (PCL): The Biodegradable Polyester Shaping the Future of Materials – a Review on Synthesis, Properties, Biodegradation, Applications and Future Perspectives. *Eur. Polym. J.* **2025**, *234* paper 114033; https://doi.org/10.1016/j.eurpolymj.2025.114033.
[17] *Nanovia HIPS as a Soluble Support Material for 3D Printing*. Nanovia; https://nanovia.tech/en/nanovia-hips-as-a-soluble-support-material-for-3d-printing/ [accessed on Oct. 10, 2025].
[18] *HIPS Filament Properties and Best Brands*. 3D Insider, **2019**; https://3dinsider.com/hips-filament/ [accessed on Oct 10, 2025].
[19] Carrot, C.; Bendaoud, A.; Pillon, C. *Handbook of Thermoplastics*. 2nd ed., CRC Press, Boca Raton, **2016**; ISBN: 978-1-4665-1886-5.
[20] Królikowski, M.; Żach, P.; Kalestyński, M. Selection of Conditions in PVB Polymer Dissolution Process for Laminated Glass Recycling Applications. *Polymers* **2022**, *14*(23) paper 5119; https://doi.org/10.3390/polym14235119.
[21] Pattinson, S.W.; Hart, A.J. Additive Manufacturing of Cellulosic Materials with Robust Mechanics and Antimicrobial Functionality. *Adv. Mater. Technol.* **2017**, *2*(4) paper 1600084; https://doi.org/10.1002/admt.201600084.
[22] *Z-SUPPORT ATP Rozpuszczalny Materiał Podporowy*. (in Polish) Zortrax; https://zortrax.com/pl/filaments/z-support-atp/ [accessed on Oct. 10, 2025].
[23] *Z-SUPPORT ATP 130*. (in Polish) Zortrax; https://zortrax.com/pl/filaments/z-support-atp-130/ [accessed on Oct. 10, 2025].
[24] *Z-SUPPORT Premium - Rozpuszczalny filament dla Zortrax Inventure*. (in Polish) Zortrax; https://zortrax.com/pl/filaments/z-support-premium/ [accessed on Oct. 10, 2025].

[25] Lu, T.; Chen, W.T. Material Recycling of Acrylonitrile Butadiene Styrene (ABS) from Toy Waste Using Density Separation and Safer Solvents. *Resour. Conserv. Recycl.* **2023**, *197* paper 107090; https://doi.org/10.1016/j.resconrec.2023.107090.
[26] *The Basics of Acrylonitrile Butadiene Styrene (ABS)*. UL Prospector; https://www.ulprospector.com/knowledge/11655/pe-the-basics-of-acrylonitrile-butadiene-styrene-abs/ [accessed on Oct. 10, 2025].
[27] *Water Soluble Sacrificial 3D Resins*. 3Dresyns; https://www.3dresyns.com/collections/water-soluble-sacrificial-3d-resins [accessed on Oct. 10, 2025].
[28] Luttrell, W.E.; Nichols, A. Ammonium Perchlorate. *J. Chem. Health Saf.* **2013**, *20*(2): 40-42; https://doi.org/10.1016/j.jchas.2013.02.005.
[29] Ayerst, R.P.; Phillips, M.I. Solubility and Refractive Index of Ammonium Perchlorate in Water. *J. Chem. Eng. Data* **1966**, *11*(4): 494-496; https://doi.org/10.1021/je60031a011.
[30] Xin, K.; Yang, R.; Yang, K.; Li, J.; Zhai, J. Hydroxyl-Terminated Polybutadiene (HTPB) Propellants Cross-Linked by Dimer Acid Diisocyanate (DDI): Cross-Linking Network and Properties. *Propellants Explos. Pyrotech.* **2024**, *49*(6) paper e202300259; https://doi.org/10.1002/prep.202300259.
[31] Liu, X.; Zhao, D.; Bi, F.; Fan, X.; Zhao, F.; Zhang, G.; Zhang, W.; Gao, Z. Synthesis, Characterization, Migration Studies and Combustion Catalytic Performances of Energetic Ionic Binuclear Ferrocene Compounds. *J. Organomet. Chem.* **2014**, *762*: 1-8; https://doi.org/10.1016/j.jorganchem.2014.03.011.
[32] Zain-ul-Abdin; Wang, L.; Yu, H.; Saleem, M.; Akram, M.; Khalid, H.; Abbasi, N.M.; Khan, R.U. Synthesis and Catalytic Performance of Ferrocene-based Compounds as Burning Rate Catalysts. *Appl. Organomet. Chem.* **2017**, *31*(11) paper e3754; https://doi.org/10.1002/aoc.3754.
[33] Quagliano Amado, J.C.; Ross, P.G.; Mattos Silva Murakami, L.; Narciso Dutra, J.C. Properties of Hydroxyl-Terminal Polybutadiene (HTPB) and Its Use as a Liner and Binder for Composite Propellants: A Review of Recent Advances. *Propellants Explos. Pyrotech.* **2022**, *47*(5) paper e202100283; https://doi.org/10.1002/prep.202100283.
[34] Willard, H.H.; Smith, G.F. The Perchlorates of the Alkali and Alkaline Earth Metals and Ammonium. Their Solubility in Water and Other Solvents. *J. Am. Chem. Soc.* **1923**, *45*(2): 286-297; https://doi.org/10.1021/ja01655a004.
[35] Brochu, S.; Ampleman, G. Synthesis and Characterization of Glycidyl Azide Polymers Using Isotactic and Chiral Poly(Epichlorohydrin)s. *Macromolecules* **1996**, *29*(17): 5539-5545; https://doi.org/10.1021/ma951839f.
[36] Eroğlu, M.S.; Baysal, B.M.; Güven, O. Determination of Solubility Parameters of Poly(Epichlorohydrin) and Poly(Glycidyl Azide) Networks. *Polymer* **1997**, *38*(8): 1945-1947; https://doi.org/10.1016/S0032-3861(96)00720-3.
[37] Bui, V.T.; Ahad, E.; Rheaume, D.; Whitehead, R. Evaluation of Branched Glycidyl Azide Polymer Purified by Solvent Extraction. *Ind. Eng. Chem. Res.* **1997**, *36*(6): 2219-2224; https://doi.org/10.1021/ie9604177.

[38] Hasegawa, K.; Takizuka, M.; Fukuda, T. Bonding Agents for AP and Nitramine/HTPB Composite Propellants. *Proc. 19th Joint Propulsion Conf.*, AIAA-1983-1199, Seattle, WA, USA, **1983**; https://doi.org/10.2514/6.1983-1199.
[39] Song, Y.; Xiao, L.; Zhou, W.; He, X. Preparation and Properties of NC/TATB/Bu-NENA/TMETN Low Sensitive Gun Propellants. *Propellants Explos. Pyrotech.* **2021**, *46*(9): 1470-1479; https://doi.org/10.1002/prep.202100147.
[40] Andersen, F.A. Amended Final Report of the Safety Assessment of Dibutyl Adipate as Used in Cosmetics. *Int. J. Toxicol.* **2006**, *25(Suppl 1)*: 129-134; https://doi.org/10.1080/10915810600716679.
[41] Schupp, T.; Plehiers, P.M. Absorption, Distribution, Metabolism, and Excretion of Methylene Diphenyl Diisocyanate and Toluene Diisocyanate: Many Similarities and Few Differences. *Toxicol. Ind. Health* **2022**, *38*(9): 500-528; https://doi.org/10.1177/07482337211060133.

Authorship contribution statement

Łukasz Mężyk:	conception, methods, performing the experimental part, performing the statistical analysis
Michal Chmielarek:	methods
Dominik Zdybał:	conception
Maciej Kołodziej:	performing the experimental part
Krzysztof Wacko:	performing the statistical analysis
Jan Kindracki:	performing the experimental part
Przemysław Woźniak:	other contribution to the publication
Sylwia Metelska:	other contribution to the publication

Submitted: October 12, 2025
Revised: December 12, 2025
First published online: December 18, 2025